Noise, morphology and control. An analysis of the stochastic behaviour of Braitenberg vehicles.

Iñaki Rañó

***Abstract*— Braitenberg vehicles are simple models of the motion of animal towards, or away from, a stimulus. They have been used to implement target reaching and avoidance behaviours in robotics, based, among others, on sound, light, distance, and pressure sensors. When the sensors are accurate enough – when they provide a high signal to noise ratio – variations on the readings can be neglected. Their behaviour, in these applications, can be explained using a non-linear deterministic dynamical system. For noisy sensors, or when the physical interaction between the robot and the measured variable is complex, a deterministic model is not good enough. Some examples include robots with cheap sensors, sensor prototypes, or settings where the interaction with the environment changes the measurements, like odour tracking – as the motion of the robot creates turbulences in the air. This paper presents the first analysis of the behaviour of Braitenberg vehicle 3a with noisy sensors. The mathematical equations of the evolution of the vehicle state probability are derived under white noise assumptions, and a bound for the vehicle state uncertainty is obtained assuming Gaussian probability distributions of the pose. These equations relate the morphological parameters of the vehicle, the noise variance and the function connecting the sensors to the actuators. The non-linear controller simulations illustrate the local validity of the model, and global simulations show how the vehicles converge.**

I. Introduction

In his seminal work [1] Valentino Braitenberg presented as a thought experiment a set of models of animal behaviour with increasing levels of complexity. These models correspond in their simpler version to the animal behaviour known as taxes, motion of animals towards (or away from) a stimulus [2]. Qualitative in nature, they are used in biology [3], although their apparent simplicity made then appealing for fields like Artificial Life [4] [5] and robotics. Whilst the descriptive version of the models are highly intuitive, its mathematical formulation has shown unreported interesting features of their behaviour like: oscillatory and bounded motion [6], or chaos [7]. The main drawback of these models is that they assume noiseless sensors, which in some cases might be unrealistic. Their validity is questionable for robots with cheap or noisy sensors, or when the robot is immersed in an environment with complex dynamics. This paper presents the first analysis of the behaviour of Braitenberg vehicle 3a in the presence of non-negligible sensor noise.

Clearly, even simpler animals master the "art" of moving in the real world. Therefore, a proper understanding of how they perform their motion would be very valuable for robotics. In fact, the principles behind a simple model like the Braitenberg vehicles has been successfully used in many robotic works. One such successful story is presented in the imitation of female cricket phonotaxis [8] [9] [10], i.e. the motion of a robot towards a sound source. A spiking neural network based model with connections following the ideas of Braitenberg vehicles achieved very good performance under quite adverse outdoor conditions. The control mechanism is comparable to a combination of vehicles 2a and 3b since excitatory neurons follow a direct connection between sensors and motors, while inhibitory units are crossed. [11] presents another implementation of phonotaxis. While the main contributions in this work are the modelling of the central auditory system in mammals (rats), and the implementation of a sound source localisation based on the pinnae and the cochlea model, the authors use the vehicle 3a principle to control their robot motion. The auditory system of a lizard is used to achieve phonotaxis in another robotic application [12]. The performance of this implementation of a lizard's ear model is good enough to work over a wide range of frequencies with a high success rate using a Braitenberg vehicle 2b and a bang-bang controller. Although the theoretical models and results of the Braitenberg vehicle 2b were not available to the authors, they were able to tune the parameters to achieve similar performance for both controllers. A wandering mechanism based on vehicle 2b is presented in [7], where the stimulus is the free area measured by the robot laser sensor. This work also shows that the motion of the vehicle 2b is equivalent to a particle in a potential well and, therefore, it can display chaotic behaviour. Finally, a vision based implementation of Braitenberg vehicles 2a and 2b was presented in [13]. The goal of this work was to imitate several reflex responses of arthropods using optical flow as a sensory input.

All of the above works can be considered to follow the deterministic models of Braitenberg vehicles. When implementing, for instance, phonotaxis, if the signal to noise ratio is high enough the noise can be neglected. On the other hand, since the readings of the laser scanners are quite accurate, in the case of the free area based wandering, the noise can also be ignored. In general that means the stochastic component of the stimulus has little influence in the behaviour. However, Braitenberg vehicles have been also used in applications with more complex stimuli. One of the pioneering works in odour source localisation [14] experimentally analysed the behaviour of Braitenberg vehicles 3a and 3b. Using two chemical sensors and normalising the readings the authors were able to direct a robot towards a chemical source or to stay near high concentrations levels. This type of application clearly differs from the ones mentioned so far. As the robot

Iñaki Rañó is with the Intelligent Systems Research Centre, Ulster University. i.rano@ulster.ac.uk

moves it induces air flows making the concentration of chemicals in the air change in potentially chaotic ways, yet this work showed that, when carefully done, Braitenberg vehicles are able to to deal with these situations. Another example of a complex vehicle is presented in [15] where a fish robot provided with pressure sensors can keep its orientation relative to a laminar flow. In this rheotaxis implementation the forward speed of the fish is kept constant, but the turning rate is computed following the principles of Braitenberg vehicles. This is another example of a situation in which the interaction between the robot and stimulus generates complex measurement patterns, and the deterministic model might not be enough to accurately describe the robot behaviour. Another application to underwater robotics worth mentioning is presented in [16], the implementation of a robotic electric fish. In this work the steering control is performed using the differences between the currents, perceived through electrodes located on the sides of the robot. The resulting trajectories approach conductive objects in a pond while avoiding isolating ones.

Through the literature we find multiple empirical applications of Braitenberg vehicles, ranging from target seeking and sound source localisation to wandering and obstacle avoidance. To characterise some of these works a deterministic model of Braitenberg vehicles might be enough. However, if the sensor readings are too noisy or the interaction between the robot and the environment produces complex variations of the measurements around some expected value – like for turbulent air flows – a model accounting for sensor noise seems more appropriate. This paper presents the first model and theoretical analysis of the motion of Braitenberg vehicle 3a for the case of noisy sensors. The theoretical analysis of the model shows interesting results linking the sensor noise, the controller and the morphological parameters of the vehicle. Therefore, this work contributes to a better understanding of this biological motion model widely used in robotics. The rest of the paper is organised as follows. Section II briefly reviews the qualitative model of Braitenberg vehicle 3a, states the working assumptions, and formally derives the model equations under sensor noise conditions. Simulations in section III illustrate the validity of the model – when the local assumptions are fulfilled – and its limits in a global situation. However we also show that the behaviour of the vehicles is globally convergent under certain conditions. Section IV ends the paper with some conclusions and future work directions.

II. A STOCHASTIC MODEL BRAITENBERG VEHICLE 3A

As stated in the introduction, Braitenberg vehicles model positive and negative taxis, i.e. motion towards, or away from, a stimulus. Vehicle 3a represents a model of positive tropo-taxis, taxis based on two sensors. Figure 1 shows the qualitative model of vehicle 3a, which has a decreasing connection between the sensors and the wheels (negative sign in the figure). The stimulus (light) source is located on the right side of the robot, which implies that the right sensor perceives a higher intensity value. A decreasing connection means that the turning velocity of the right wheel will be smaller than the one for the left wheel, making the vehicle effectively head towards the (light) source. Therefore, one of the implicit assumptions in the original qualitative work [1] is that there is a purely kinematic relation between the sensors and the actuators. While wheels abstract the locomotive system of animals, they also capture the fact that their motion is non-holonomic, which is a good approximation especially for high speeds.

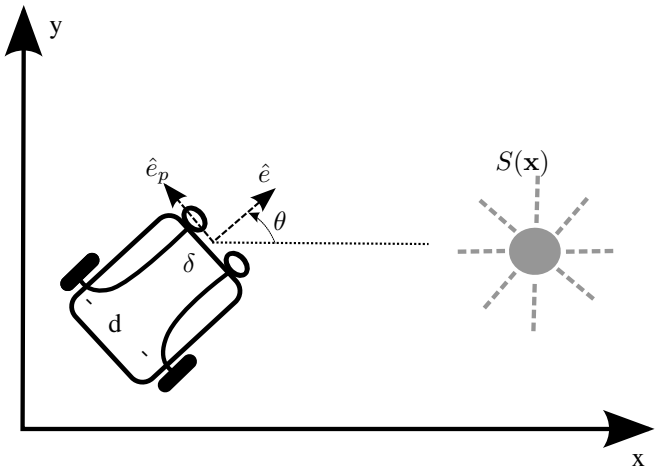

Fig. 1. Braitenberg vehicle 3a

A. Linear and angular velocities uncertainty

Following figure 1, we will assume the state of the vehicle can be described by the Cartesian coordinates of the midpoint between the sensors $\mathbf{x} = (x, y)$, and its heading direction θ. We will also assume that there is a position dependent stimulus which can be modelled as a smooth function $S(\mathbf{x})$. If the stimulus comes for instance from a light or sound source, its intensity – what we expect the sensor to measure – decays with the square of the distance, i.e. it follows the inverse square law. In general, however, the function $S(\mathbf{x})$ does not need to be a real stimulus, it could represent an artificial potential or even a function of a group of sensor readings, like the free area around the robot used in [7]. We will assume the stimulus is the combination of a deterministic function $S_0(\mathbf{x})$ and some white random noise following a Gaussian distribution, $S(\mathbf{x}) = S_0(\mathbf{x}) + \eta$, where $\eta \sim \mathcal{N}\left(0, \sigma_\eta^2\right)$. It is worth reminding that the deterministic function can have any profile, depending on the stimulus used, but we will assume it is a smooth enough function of the position $\mathbf{x}$.

Using the same notation as for the deterministic model of vehicle 3a [17] we define an orthonormal reference system linked to the front of the vehicle $\{\hat{e}, \hat{e}_p\}$. These vectors are defined by the heading direction of the vehicle θ (see figure 1) as $\hat{e}^T = [\cos\theta \ \ \sin\theta]$ and $\hat{e}_p^T = [-\sin\theta \ \ \cos\theta]$. We will further assume that the relation between the measured stimulus and the speeds of the wheels is purely functional, i.e. $v = F(s)$, where s is the sensor measurement and v the linear velocity of the wheel axis. The fact that this vehicle

has a decreasing connection constrains the possible functions to have a negative slope in the range of the sensor readings, i.e. $F'(s) < 0$. This also implies that $F(s)$ has to be at least C^1, but for convenience we will assume $F(s) \in C^\infty$. It is worth noting that there is no linearity constraint on the function and, therefore, the wheel speeds might not follow a Gaussian distribution. Under these assumptions, the speeds of the right and left wheels can be stated as:

$$\begin{aligned} v_r &= F(S(\mathbf{x} - \frac{\delta}{2}\hat{e}_p)) \\ v_l &= F(S(\mathbf{x} + \frac{\delta}{2}\hat{e}_p)) \end{aligned} \quad (1)$$

where δ is the distance between the vehicle sensors (see figure 1). We can linearise $F(s)$ and approximate the wheel speeds as $v_r \sim \mathcal{N}\left(F_r, [F_r']^2 \sigma_\eta^2\right)$ and $v_l \sim \mathcal{N}\left(F_l, [F_l']^2 \sigma_\eta^2\right)$, where F_r, F_l, F_r' and F_l' are the compound function $F(S_0(\mathbf{x}))$ and its derivative evaluated at the corresponding sensor locations $\mathbf{x}_r = \mathbf{x} - \frac{\delta}{2}\hat{e}_p$ and $\mathbf{x}_l = \mathbf{x} + \frac{\delta}{2}\hat{e}_p$. If we now use the standard linear transformation between wheel velocities (v_r and v_l) and the forward speed v and turning rate ω of the vehicle, they approximately follow the distributions $v \sim \mathcal{N}\left(\frac{F_r+F_l}{2}, \frac{\sigma_\eta^2}{4}[[F_r']^2 + [F_l']^2]\right)$ $\omega \sim \mathcal{N}\left(\frac{F_l-F_r}{d}, \frac{\sigma_\eta^2}{d^2}[[F_r']^2 + [F_l']^2]\right)$, where, as figure 1, d is the vehicle wheelbase.

Since we imposed smoothness conditions for the stimulus function $S_0(\mathbf{x})$ and for $F(s)$, we can approximate the function composition around the middle point between the sensors as:

$$F_l \approx F(S_0(\mathbf{x})) + \frac{\delta}{2}F'(S_0(\mathbf{x}))\nabla S_0(\mathbf{x}) \cdot \hat{e}_p \quad (2)$$

$$F_r \approx F(S_0(\mathbf{x})) - \frac{\delta}{2}F'(S_0(\mathbf{x}))\nabla S_0(\mathbf{x}) \cdot \hat{e}_p \quad (3)$$

where $F'(s)$ represents the derivative of $F(s)$ w.r.t. 's' and $\nabla S_0(\mathbf{x})$ is the gradient of the deterministic component of the stimulus function. The corresponding derivatives can be also approximated as:

$$F_l' \approx F'(S_0(\mathbf{x})) + \frac{\delta}{2}F''(S_0(\mathbf{x}))\nabla S_0(\mathbf{x}) \cdot \hat{e}_p \quad (4)$$

$$F_r' \approx F'(S_0(\mathbf{x})) - \frac{\delta}{2}F''(S_0(\mathbf{x}))\nabla S_0(\mathbf{x}) \cdot \hat{e}_p \quad (5)$$

where $F''(s)$ is the second derivative of $F(s)$ w.r.t. 's'. If we substitute equations (2), (3), (4) and (5) in the expressions for the mean and covariances of the linear and angular speeds of the vehicle, we get:

$$v \sim \mathcal{N}\left(F, \frac{\sigma_\eta^2}{2}\rho\right) \quad (6)$$

$$\omega \sim \mathcal{N}\left(-\frac{\delta}{d}F'\nabla S_0 \cdot \hat{e}_p, \frac{2\sigma_\eta^2}{d^2}\rho\right) \quad (7)$$

where $F = F(S_0(\mathbf{x}))$ is the function evaluated at the stimulus value of the middle point between the sensors, $F' = F'(S_0(\mathbf{x}))$ is its derivative, $\nabla S_0 = \nabla S_0(\mathbf{x})$ is the gradient of the stimulus at that point, and

$$\rho = [F']^2 + \frac{\delta^2}{2}\left[F''\nabla S_0 \cdot \hat{e}_p\right]^2 \quad (8)$$

Obviously, the expressions obtained for average speeds are the same as for the deterministic model of vehicle 3a [17], yet the equations of the variances show interesting results. It is straightforward to see that the noise variance σ_η^2 has a direct effect on the variances of both variables, linear and angular speeds. However, equation (7) shows that to reduce the overall effect of the noise on the angular velocity, the vehicle requires a large wheelbase d. This has an intuitive explanation if we consider the mean value of the vehicle turning rate. The change in the direction is driven by the directional derivative of the stimulus in the direction orthogonal to the vehicle, the mean in the equation (7). Because the angular velocity is $\omega = \frac{v_l - v_r}{d}$, increasing the wheel base reduces the turning rate, and this has the effect of decreasing the variance σ_ω^2. Therefore, the model provides a relation between the vehicle morphological parameter d, the variance of the sensor noise, and the parameters of the non-linear controller $F(s)$. It is worth noting that the variance of the turning rate depends on the direction the vehicle is heading, such that it has its minimum when it is aligned with the gradient of $S(\mathbf{x})$, either the same or opposite directions.

B. Time evolution of the trajectories

From the probability distributions of the speeds, equations (6) and (7) we can derive the evolution of the state of the Braitenberg vehicle 3a. Its kinematics correspond to the well known unicycle motion model, a non-linear non-holonomic system which in its discrete form can be written as:

$$\begin{bmatrix} x_{k+1} \\ y_{k+1} \\ \theta_{k+1} \end{bmatrix} = \begin{bmatrix} x_k + \Delta T v_k \cos\theta_k \\ y_k + \Delta T v_k \sin\theta_k \\ \theta_k + \Delta T \omega_k \end{bmatrix} \quad (9)$$

where $\mathbf{X}_k = [x_k, y_k, \theta_k]$ is the state of the vehicle at time-step k, v_k and ω_k are the linear and angular speeds, and ΔT is the sampling discretisation time. Through these equations we can obtain the evolution of the vehicle over time. Since we have a model of the control variables as a Gaussian probability, we can compute an approximation of the distribution of the state at $k+1$ if we assume the probability distribution of the state of the system at time k is Gaussian $p(\mathbf{X}_k) \sim \mathcal{N}(\mu_{\mathbf{X}_k}, \Sigma_{\mathbf{X}_k})$, where $\mu_{\mathbf{X}_k}$ is the average of the state, and $\Sigma_{\mathbf{X}_k}$ its covariance matrix. Obviously, because the unicycle system's equations are non-linear, the resulting distribution will not be Gaussian, but we can linearise equation (9) to get an approximation and we obtain a closed form solution for the probability $p(\mathbf{X}_{k+1})$. Moreover, due to the topology of the state space it might be more appropriate to model the heading direction as a

von Mises distribution, but we will follow the standard assumption of Gaussianity over the pose.

The mean of the $p(\mathbf{X}_{k+1})$ distribution $\mu_{\mathbf{X}_{k+1}}$ can be easily computed plugging $\mu_{\mathbf{X}_k}$ in equations (9), while the covariance matrix $\Sigma_{\mathbf{X}_{k+1}}$ is obtained from linearised equations of the system as:

$$\Sigma_{\mathbf{X}_{k+1}} \quad = \quad \Sigma_{\mathbf{X}_k} + J_{\mathbf{X}_k}\Sigma_{\mathbf{X}_k}J_{\mathbf{X}_k}^T + J_{\mathbf{u}_k}\Sigma_{\mathbf{u}_k}J_{\mathbf{u}_k}^T \quad (10)$$

where we define the control input vector $\mathbf{u}_k = [v_k, \omega_k]$, which follows a two dimensional Gaussian distribution $\mathbf{u}_k \sim \mathcal{N}(\mu_{\mathbf{u}_k}, \Sigma_{\mathbf{u}_k})$, with $\mu_{\mathbf{u}_k}$ the vector of means from equations (6) and (7), and $\Sigma_{\mathbf{u}_k}$ a diagonal matrix with the variances from equations (6) and (7). The matrices $J_{\mathbf{X}_k}$ and $J_{\mathbf{u}_k}$ are the Jacobians of the evolution equation (9) with respect to the state and the control input respectively, which have the following form:

$$J_{\mathbf{X}_k} = \begin{bmatrix} 0 & 0 & -\Delta T v_k \sin\theta_k \\ 0 & 0 & \Delta T v_k \cos\theta_k \\ 0 & 0 & 0 \end{bmatrix}$$

and

$$J_{\mathbf{u}_k} = \begin{bmatrix} \Delta T \cos\theta_k & 0 \\ \Delta T \sin\theta_k & 0 \\ 0 & \Delta T \end{bmatrix}$$

In general, for the deterministic equations – which coincides with the average behaviour of the vehicle – the trajectory the robot will follow can be quite complex. It is in fact the solution to a set of non-linear differential equations. However, for some specific stimulus functions analytic solutions can be found. Simple solutions to motion include circular trajectories or spirals around a circularly symmetric stimulus source [17], or straight line trajectories for circular symmetry or compound functions of parabolas (stimulus of the type $S(\mathbf{x}^T A\mathbf{x})$ with A a positive definite matrix) [6]. This latter case occurs when the robot is aligned with one of the principal directions of the parabola. If it heads the source it will follow a straight line trajectory with variable linear speed ending at the stimulus maximum. The robot will follow a straight line trajectory moving away from the maximum of $S(\mathbf{x})$ if the source is on its back. We can use these simple average trajectories to analyse the behaviour of the stochastic model. Assuming without loss of generality that the maximum of $S(\mathbf{x})$ is at the origin, and the vehicle lies on the negative side of the 'x' axis with an initial heading $\theta_0 = 0$, the average trajectory for a circularly symmetric ($S(r)$, with $r^2 = |\mathbf{x}|^2$) or parabolic stimulus ($S(\mathbf{x}^T D\mathbf{x})$ with D a diagonal positive definite matrix) will be a straight line, and the Jacobian matrices in equation (10) will simplify. Under these assumptions the initial covariance matrix of the state of the vehicle is simply a zero matrix $\Sigma_{\mathbf{X}_0}$, and the recursive estimation of the covariance using equation (10) leads to:

$$\Sigma_{\mathbf{X}_k} = T^2\sigma_\eta^2 \begin{bmatrix} \frac{1}{2}\sum_{i=0}^{k-1}[F_i']^2 & 0 & 0 \\ 0 & \frac{2T^2}{d^2}\sum_{i=1}^{k-1}[F_i]^2\sum_{j=0}^{i-1}[F_j']^2 & 0 \\ 0 & 0 & \frac{2}{d^2}\sum_{i=0}^{k-1}[F_i']^2 \end{bmatrix}$$

where $F_i = F(S_0(\mathbf{x}_i))$ and $F_i' = F'(S_0(\mathbf{x}_i))$, since for the selected scenario the gradient of $S_0(\mathbf{x})$ is orthogonal to $\hat{e}_p$, simplifying the expression (8) to $\rho = [F']^2$. Given our continuity assumption on $F(s)$, the function will also be Lipschitz continuous, which means a bound value m for its derivative exists, but also a bound f for the $F(s)$ function itself within the domain. This condition helps in finding a boundary to the state covariance matrix under our assumptions, and therefore:

$$\Sigma_{\mathbf{X}_k} \quad < \quad T^2\sigma_\eta^2 m^2 \begin{bmatrix} \frac{k}{2} & 0 & 0 \\ 0 & \left[\frac{fT}{d}\right]^2 k(k+1) & 0 \\ 0 & 0 & \frac{2k}{d^2} \end{bmatrix} \quad (11)$$

where the $<$ sign applies to the elements of the diagonal matrix. This limit shows interesting properties of the evolution of the state probability. First, our assumptions imply that the state variables are uncorrelated, since all the off-diagonal elements of the matrix are zero for this specific solution. More importantly, while the variance of the x position and the vehicle heading θ grows linearly with time, the dispersion in the y direction grows as a quadratic function of time. Moreover, the variance in the y coordinate depends on the variance of the angular velocity σ_ω^2. This is not a surprising result given the trajectory we are analysing, as the heading integrates the angular velocity and the linearised equation for y integrates the heading ($\dot{y} \approx v\theta$). In general, if the robot heads the target along one of the principal directions – or radially for circular symmetry – the growth of the variance in the direction orthogonal to the vehicle motion will be a quadratic function of time, while it will be linear for the heading and the direction of motion.

C. Remarks on the resulting model

One interesting result of the above equations is the fact that the speed variances depend on the direction of motion of the vehicle, but also on the second derivative of the function $F(s)$, see equation (6)-(8). What equation (8) tells is that to minimise the variance of both control variables, one good option is to choose a linear $F(s)$, since its second derivative vanishes for all 's'. This is a very interesting result which helps in understanding and justifies, for instance, why in [14] the authors selected a linear connection between the sensors and the actuators. Besides being the simplest option, a linear $F(s)$ achieves a minimum variance of the speeds in noisy situations (in the case of [14] when the stimulus changes are linked to the robot motion in a complex way). Likewise, if we select a linear function $F(s) = as + b$, we could eventually reduce the variances to zero for $a = 0$. This is the limit case

in which the sensors are disconnected from the motors and, therefore, the vehicle will not move, which trivially leads to a zero variance of the speeds.

In order to minimise the dispersion of the vehicle trajectories a low value of $F'(s)$ is required. However, if we consider the stability condition [17] obtained for a circularly symmetric stimulus in the deterministic (average) case:

$$\frac{F}{r} - \frac{\delta}{d} F' \frac{\partial S}{\partial r} < 0$$

where r is the distance to the stimulus source, and $S(\cdot)$ is just a function of r, we can rewrite this condition as $\frac{F'}{d} > \frac{F}{r\delta S_r}$, with $S_r = \frac{\partial S}{\partial r}$. This sets a convergence limit to the ratio $\frac{F'}{d}$, and if its value is too low the vehicle will not reach the target. It can be seen that for a linear $F(s)$, $\sigma_\omega^2 \propto \left[\frac{F'}{d}\right]^2$ and therefore the selection of $F(s)$ requires to have small enough $\frac{F'}{d}$ to minimise the dispersion of the vehicle heading, but large enough for it to converge to the goal, the maximum of $S(\mathbf{x})$.

III. Simulations

This section presents simulations of Braitenberg vehicles to illustrate the derived stochastic evolution model of vehicle 3a. We compare the analytical results with simulations of $1,000$ vehicles moving in the corresponding conditions following to the discretised unicycle model, equation (9). We also present simulations of global behaviour of this Braitenberg vehicle to show the general convergence properties of the controller in a noisy environment.

Figure 2 shows the simulation of a Braitenberg vehicle 3a starting with poses $x_0 = -3$ (fig. 2(a)), $x_0 = -1.5$ (fig. 2(a)), $y_0 = 0$ and $\theta_0 = 0$. The stimulus consists of a parabolic shaped function with the peak at the origin, and $F(s)$ is simply a linear function of 's' with negative slope. Therefore, the compound function is $F(S(\mathbf{x})) = \alpha[g_0 - \mathbf{x}^T A \mathbf{x}] + \beta$, for $g_0 > 0$, A positive definite, $\alpha < 0$, and such that $F(S(0)) = 0$. This type of stimulus can be always used as an approximation close enough to a smooth stimulus peak. As the plots show, the average trajectory follows a straight line towards the origin. The figures show the average model trajectory – continuous line – and the simulated trajectory – dashed line. Only six steps of equation (9) were simulated to illustrate the theoretical results, and, as it can be seen, all the simulated vehicles started with the same pose, i.e. the probability distribution $p(\mathbf{X}_0)$ is a Gaussian with zero covariance matrix. The theoretical covariance matrix was computed iteratively for each step, and the maximum values of $F(s)$ and $F'(x)$ (f and m) at the simulated points were used to obtain the covariance bound matrix, equation (11). Figures show the '$x - y$' components of the covariances ($\pm\sigma$) at each position of the vehicle, with the dotted ellipses corresponding to the theoretical bound. As we can see from the figures the sampled trajectory coincides quite well with the theoretical one, both the mean – the horizontal line – and covariance – ellipses around the simulated points. Comparing the dispersion on the 'y' direction of figures 2(a) and 2(b) we can see several interesting effects. It is worth noting that the linear speed decreases as the vehicle approaches the stimulus source, which means that the points $\{x_0, x_1, \cdots, x_7\}$ are closer to each other for the starting position $x_0 = -1.5$. That has an effect on how the '$x - y$' covariance matrix spreads over the 'y' direction, since a higher forward speed implies a higher σ_y^2 in equation (11), which is reflected in the 'y' range of the plots. On the other hand, that also means that as the vehicle gets closer to the origin its variance in the perpendicular direction to motion does not grow so fast. Therefore, the covariance boundary matrix becomes less conservative as the vehicle approaches the target, as shown by the fact that the dotted lines are closer to the theoretical value in figure 2(b).

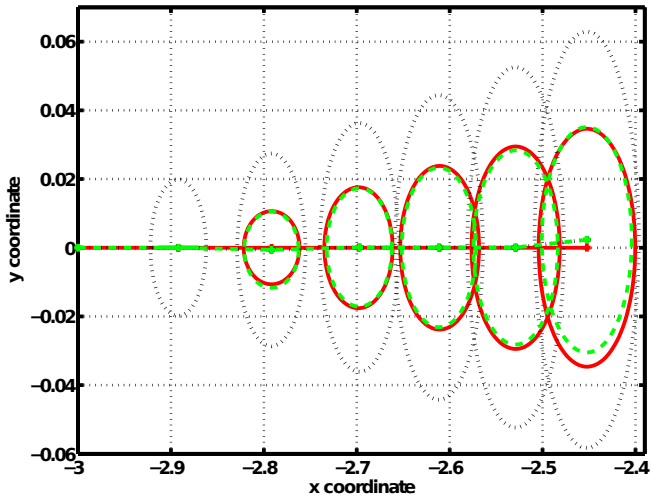

(a) Starting point $x = -3$

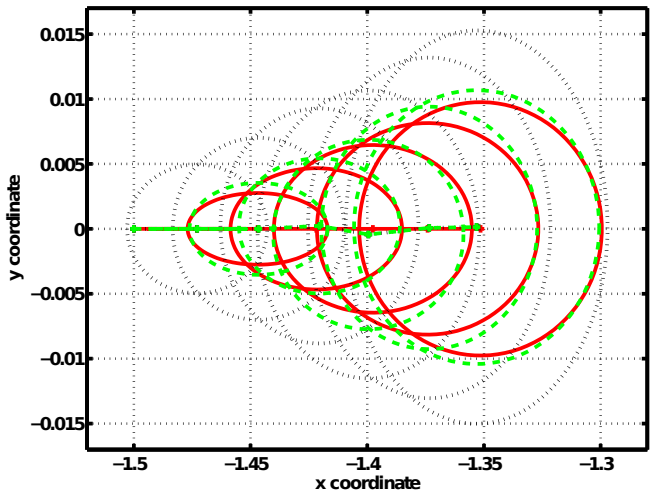

(b) Starting point $x = -1.5$

Fig. 2. Simulated stochastic vehicle for a parabolic $S(\mathbf{x})$ and linear $F(s)$

Although the simulations match the theoretical results and help to understand the behaviour of vehicles in presence of noise, because of the locality of the assumptions the global behaviour is not captured by the model. It would seem, looking at equation (11), that the covariance of the vehicles always increases, yet globally, as illustrated in Figure 3, the

opposite actually happens. The figure shows a simulation of vehicles initialised randomly over the '$x - y$' plane according to a Gaussian distribution. In this case the stimulus follows an inverse square law $S(\mathbf{x}) = \frac{g_0}{1+\alpha \mathbf{x}^T A \mathbf{x}}$ and $F(s)$ is linear. Each vehicle initially points towards the origin – the peak of $S(\mathbf{x})$ – with a random deviation following a Gaussian distribution. The nearly concentric ellipses show the evolution of the covariance of the simulated vehicles, while the line close to the origin is the average position, which ideally should be zero. The outer ellipse in the figure corresponds to the initial pose distribution of the vehicles around the origin (within $\pm\sigma$). Because it is common to let the vehicles move only forward, if one of the simulated vehicles has a negative velocity for its wheels, it is set to zero. The figure shows that the dispersion of the simulated vehicles decreases, something the model is not able to predict since, for instance, a zero average of the heading direction means that the vehicles move parallel to the x axis (yet in this case is clearly at the origin). This zero mean effect occurs in this simulation, although the distribution of vehicle directions is uniform, which implies the average of the angle is not properly defined. Figure 3 shows that vehicles 3a actually move towards the goal despite the noisy sensors.

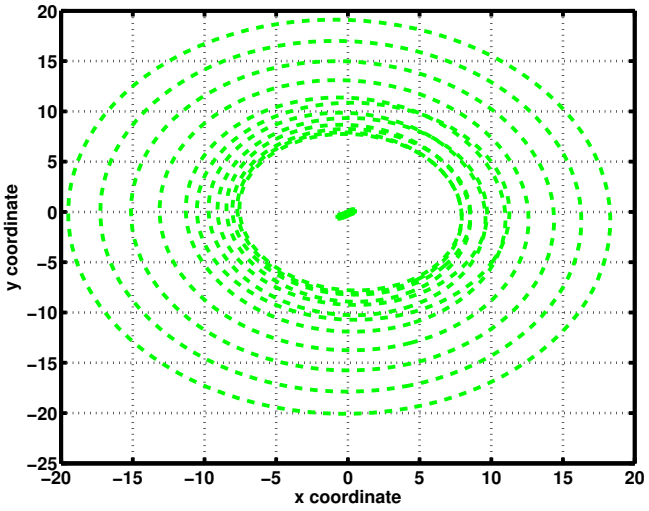

Fig. 3. Evolution of a Gaussian distribution over time of vehicles in $x - y$

IV. Conclusions and Further Work

This paper presents the first model and analysis of Braitenberg vehicles under sensor noise conditions. The existing deterministic model seems suitable to understand and design controllers for non-holonomic vehicles with good signal to noise ratio. However, for very noisy sensors or complex interactions between the robot and the environment, e.g. chemical sensing in air or water, a deterministic approach seems unsuitable. Using the derived model and existing stability conditions, we showed that there is a trade-off between stability and noise through the control function $F(s)$ and the wheelbase d. Specifically, an increase in the ratio $\frac{F'}{d}$ makes the vehicle more stable on average, but also increases the vehicle state covariance. Another interesting result from the presented analysis is that the best controller for this taxis model – in terms of the dispersion it generates – is actually a linear relation between the sensors and the motors. This has interesting implications for robotics, but also for biology. Coincidentally, this type of connection was the one used for a Braitenberg vehicle with a complex stimulus pattern [14].

As shown in section III the working range of the model is limited by the matching assumptions, as it can only explain local behaviour. Our goal is to extend this model and analyse globally the behaviour of these vehicles using Monte Carlo simulations. The model can also be extended to other Braitenberg vehicles, like vehicle 2b, which can display chaotic behaviour. The analysis of this vehicle would turn to be much more complex, as it might be a mixture of chaos and randomness.

References

[1] V. Braitenberg, *Vehicles. Experiments in synthetic psychology*. The MIT Press, 1984.

[2] G. Fraenkel and D. Gunn, *The orientation of animals. Kineses, taxes and compass reactions*. Dover publications, 1961.

[3] A. Gomez-Marin, B. Duistermars, M. Frye, and M. Louis, "Mechanisms of odor-tracking: Multiple sensors for enhanced perception and behavior," *Frontiers in Cellular Neuroscience*, vol. 4, 2010.

[4] M. Resnik, "LEGO, Logo and Life," in *Artificial Life. Proceedings of an Interdisciplinary Workshop on the Synthesis and Simulation of Living Systems*, 1987, pp. 397–406.

[5] M. Travers, "Animal construction kits," in *Artificial Life. Proceedings of an Interdisciplinary Workshop on the Synthesis and Simulation of Living Systems*, 1987, pp. 421–442.

[6] I. Rañó, "Results on the convergence of braitenberg vehicle 3a," *Artificial Life*, vol. 20, no. 2, pp. 223–235, 2014.

[7] ——, "The bio-inspired chaotic robot," in *Proc. of the IEEE International Conference on Robotics and Automation*, 2014, pp. 304–309.

[8] B. Webb, *A Spiking Neuron Controller for Robot Phonotaxis*. The MIT/AAAI Press, 2001, pp. 3–20.

[9] A. Horchler, R. Reeve, B. Webb, and R. Quinn, "Robot phonotaxis in the wild: a biologically inspired approach to outdoor sound localization," *Advanced Robotics*, vol. 18, no. 8, pp. 801–816, 2004.

[10] R. Reeve, B. Webb, A. Horchlerb, G. Indiveri, and R. Quinn, "New technologies for testing a model of cricket phonotaxis on an outdoor robot," *Robotics and Autonomous Systems*, vol. 51, no. 1, pp. 41–54, 2005.

[11] M. Bernard, S. N'Guyen, P. Pirim, B. Gas, and J.-A. Meyer, "Phonotaxis behavior in the artificial rat psikharpax," in *International Symposium on Robotics and Intelligent Sensors, IRIS2010*, 2010.

[12] D. Shaikh, J. Hallam, J. Christensen-Dalsgaard, and L. Zhang, "A Braitenberg lizard: Continuous phonotaxis with a lizard ear model," in *Proceedings of the 3rd International Work-Conference on The Interplay Between Natural and Artificial Computation*, 2009, pp. 439–448.

[13] D. Blustein and J. Ayers, "A conserved network for control of arthropod exteroceptive optical flow reflexes during locomotion," in *From Animals to Animats. Lecture Notes in Computer Science*, vol. 6226, 2010, pp. 72–81.

[14] A. J. Lilienthal and T. Duckett, "Experimental analysis of gas-sensitive Braitenberg vehicles," *Advanced Robotics*, vol. 18, no. 8, pp. 817–834, 2004.

[15] T. Salumäe, I. Rañó, O. Akanyeti, and M. Kruusmaa, "Against the flow: A braitenberg controller for a fish robot," in *Proceedings of the International Conference on Robotics and Automation (ICRA)*, 2012, pp. 4210–4215.

[16] V. Lebastard, F. Boyer, C. Chevallereau, and N. Servagent, "Underwater electro-naviagation in the dark," in *Proceedings of the International Conference on Robotics and Automation (ICRA)*, 2012, pp. 1155–1160.

[17] I. Rañó, "A steering taxis model and the qualitative analysis of its trajectories," *Adaptive Behavior*, vol. 17, no. 3, pp. 197–211, 2009.